Scripta Materialia 116 (2016) 95–99

Contents lists available at ScienceDirect

Scripta Materialia

journal homepage: www.elsevier.com/locate/scriptamat

Sample size effects on strength and deformation mechanism of $Sc_{75}Fe_{25}$ nanoglass and metallic glass

Xiaolei Wang [a], Feng Jiang [a,*], Horst Hahn [b,e,f], Ju Li [c,d], Herbert Gleiter [b,e], Jun Sun [a], Jixiang Fang [a,*]

[a] State Key Laboratory for Mechanical Behavior of Materials, School of Materials Science and Engineering, School of Science, Xi'an Jiaotong University, Xi'an 710049, China
[b] Institute for Nanotechnology, Karlsruhe Institute of Technology (KIT), 76021 Karlsruhe, Germany
[c] Department of Nuclear Science and Engineering, MIT, Cambridge, MA 02139, USA
[d] Department of Materials Science and Engineering, MIT, Cambridge, MA 02139, USA
[e] Herbert Gleiter Institute of Nanoscience, Nanjing University of Science and Technology, Nanjing 210094, China
[f] Joint Research Laboratory Nanomaterials (KIT-TUD), TU Darmstadt, 64287 Darmstadt, Germany

ARTICLE INFO

Article history:
Received 10 January 2016
Accepted 23 January 2016
Available online 10 February 2016

Keywords:
Nanoglasses
Metallic glasses
In-situ
Strength
Shear band nucleation

ABSTRACT

The mechanical properties and deformation mechanism of $Sc_{75}Fe_{25}$ nanoglass and $Sc_{75}Fe_{25}$ metallic glass pillars with diameter from 2 μm to 95 nm were investigated by means of ex-situ and in-situ compression tests. The results showed that the yield strength and deformation mechanism in the metallic glass were size-dependent while these in the nanoglass were not. It is suggested that the reduced shear band nucleation sites in metallic glass with decreasing sample size results in the increased yield strength and transition of deformation mode. In contrast, the glass/glass interfaces in nanoglass which have reduced density could serve as shear band nucleation sites and therefore promote multiple shear banding.

Nanoglasses which were conceived by H. Gleiter in 1989 [1] are amorphous solids that consist of nanometer-sized glassy regions connected by glass/glass interfaces (GGIs) with an amorphous structure. In the past two decades, nanoglasses presented attractive physical properties [2], remarkable biocompatibility [3] and excellent mechanical properties due to the their unique microstructure [4]. These novel features of nanoglasses might open the way for new technological applications in the field of micro-electro-mechanical systems (MEMS). It is well known that the strength and plastic deformation mode of most materials changes significantly when the overall physical dimensions decreases to the micro- or nano-scales [5–15]. However, there has not been a systematic study on the mechanical properties of nanoglasses in this scale. In this paper, $Sc_{75}Fe_{25}$ (at.%) nanoglass and metallic glass with identical chemical composition were selected to be the model material. Their mechanical properties and deformation mechanism were investigated by means of quantitative ex-situ compression tests on micron-sized samples as well as in-situ compression tests inside a transmission electron microscope (TEM) on submicron-sized samples. The current report attempts to provide an answer to the question is there a size effect of strength and deformation mechanism in nanoglasses (See Table 1).

The $Sc_{75}Fe_{25}$ nanoglass sample was produced by inert-gas condensation (IGC) and the metallic glass as a ribbon was produced by melt-spinning, respectively [16]. A set of micrometer-sized columnar pillars (diameter ≈2 μm) and submicron-sized square taper-free pillars (with nominal sizes of 300 nm, 160 nm and 95 nm, respectively) were successfully fabricated, using a FEI Helios NanoLab 600i dual-beam FIB system. The detailed fabrication process was the same as that in Ref. [4]. The 2 μm columnar pillars with aspect ratio (h/d) of 2.5 and sidewall tapering angle lower than 3° were tested by ex-situ compression using a nanoindenter (TI950, Hysitron) with a diamond flat conical tip. The minimum diameters at the top of pillars were used as their nominal sizes. For in-situ tests, the shape of submicron-sized pillars was taper-free with a square cross section and an aspect ratio of ~2. In practice, the cross section of the taper-free samples would be a trapezoid rather than a square due to the FIB processing. The square roots of the cross section area of the samples were calculated and were used as their nominal sizes. In-situ compression experiments were performed inside the chamber of a JEOL JEM-2100F TEM, using a Hysitron PI95 TEM PicoIndenter with a 2 μm diamond flat punch. These test method and parameter were also same as in Ref. [4].

Fig. 1a shows the compressive stress–strain curves of pillars for the nanoglass. The 2 μm nanoglass pillar exhibited nonlinear plasticity after the yield point and working hardening. At the beginning of the deformation process, the stress–strain relationship was linear. The pillar was noted to yield with a stress of ~1.34 GPa. Subsequently it hardens and finally fractures at a stress of ~1.87 GPa (Fig. 1a(I)). The total plastic

* Corresponding authors.
E-mail addresses: jiangfeng@mail.xjtu.edu.cn (F. Jiang), jxfang@mail.xjtu.edu.cn (J. Fang).

http://dx.doi.org/10.1016/j.scriptamat.2016.01.036
1359-6462/

Table 1
Movies of in-situ compression tests.

	Samples
Movie 1	300 nm nanoglass
Movie 2	160 nm nanoglass
Movie 3	95 nm nanoglass
Movie 4	300 nm metallic glass
Movie 5	160 nm metallic glass
Movie 6	95 nm metallic glass

All the movies are speeded up by 5 times.

strain prior to failure was ~3%. In the micrographs, multiple shear bands were observed at the free surface of the nanoglass (Fig. 1b(I)). When the sample size was reduced to the sub-micron regime, in situ compression tests were performed in a TEM. For the 300 nm nanoglass sample, the initial linear elastic deformation is followed by a plastic yield (Fig. 1a(II)). As the plastic deformation process went on, the stress increased to about 1.7 GPa until the test was stopped at a pre-selected strain of 20%. Numerous small stress drops with amplitudes of less than 0.1 GPa were noted during the deformation. Although not every shear band can be identified in the movie, these stress drop likely originated from the propagation of a large number of small shear bands [17]. The nanoglass sample deformed relatively uniformly due to multiple shear band mechanism rather than localized shear and its size (in the transversal direction) increased as shown in Movie 1. When the sample size was reduced to 160 nm, the nanoglass still displayed a deformation mode that was similar to the ones reported above for the 300 nm sample: an initially linear uniform elastic deformation was followed by a uniform plastic deformation with a plastic strain of about 24% and a stress of 2.4 GPa when the test was stopped at a pre-selected strain of 30%. The appearance of stress drops with amplitudes of 0.2–0.7 GPa (Fig. 1a(III)) indicated discrete shear band formation (Movie 2). The localized deformation was also apparent in the case of the deformed sample (Fig. 1b(III)). Plastic deformation would continue if compression tests were not interrupted for them. When sample size reduced to less than 100 nm, a uniform deformation mode (Fig. 1a(IV) and Fig. 1b(IV)) was noted in nanoglass. 95 nm nanoglass displayed a uniform plastic deformation with a plastic strain of about 40% and a stress of 2.6 GPa when the test was stopped at a pre-selected strain of 50% (Movie 3). The pillar presented an enhanced plastic deformation strain and higher fracture strength. It is suggested that the nanoglass displayed a tendency for deformation mode transition when the sample size reduced to <100 nm.

Fig. 2a shows the compressive stress–strain curves of pillars for the metallic glass. The 2 μm metallic glass pillar deformed like a brittle material and exhibited purely elastic behavior up to a fracture stress of ~1.84 GPa followed by catastrophic failure (corresponding to the stress burst in Fig. 2a(I)) at ~4% strain. In the postmortem SEM observation, only one single shear band appeared at the surface of the fractured pillar (Fig. 2b(I)) which is contrary to the nanoglass with similar size. For the 300 nm metallic glass, after the initial elastic deformation, it deformed continuously until a large stress drop with an amplitude of ~0.4 GPa occurred (Fig. 2a(II)). This stress drop was correlated with an obvious shear offset appearing on the free surface, followed by three subsequent stress drops associated with the formation of shear bands. Finally, the 300 nm pillar failed along the plane of largest shear band (Movie 4). Although the 300 nm metallic glass pillar still failed by shear banding, it was more ductile than the micron-sized sample.

For 160 nm metallic glass, plastic flow was relatively homogeneous [18,19] as shown in Fig. 2a(III) and Movie 5. After an initial uniform linear deformation (~4%), plastic deformation was noted (Fig. 2a(III)) without large drops of the stress. At a plastic strain of ~9%, a stress drop of ~0.15 GPa occurred. This drop was much smaller than the one of the metallic glass sample with a larger size of 300 nm (0.4 GPa). During the subsequent plastic deformation process, many stress drops with small amplitudes appeared until the sample failed catastrophically by shear with a total plastic strain of ~22% (Movie 5) at a fracture stress of ~2.3 GPa. The compression test of 95 nm metallic glass pillar was stopped at a preset strain of 50% resulting in a drum shaped pillar. The entire deformation process could be seen in Movie 6. From these observations, it is clearly concluded that the decreasing sample size (from 2 μm down to 95 nm) of a rapidly-quenched metallic glass reduces

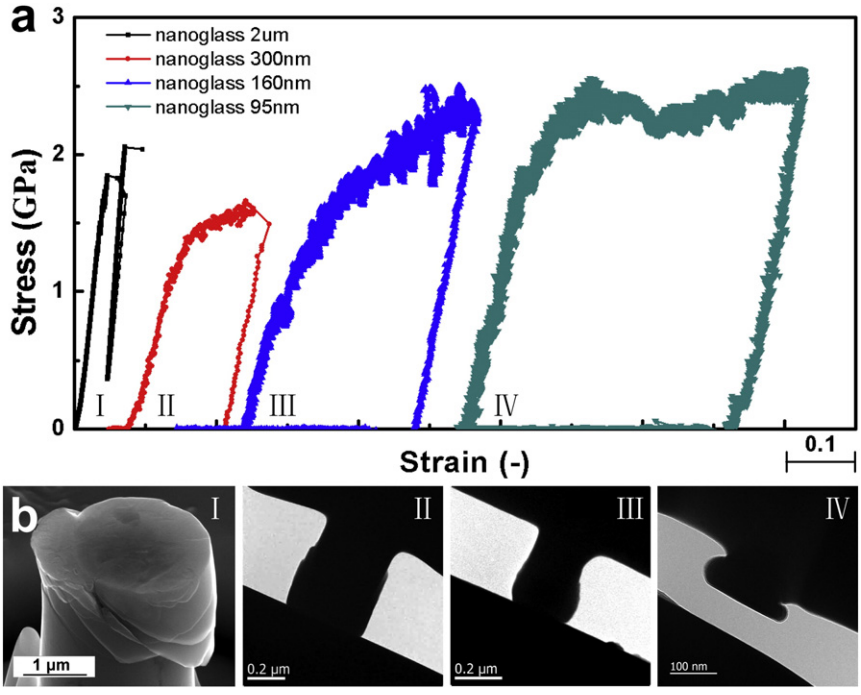

Fig. 1. (a) The compressive stress–strain curves of $Sc_{75}Fe_{25}$ nanoglass pillars. (b) The frames of (I) 2 μm; (II) 300 nm; (III) 160 nm; (IV) 95 nm nanoglass pillar, respectively, are extracted from recorded movies.

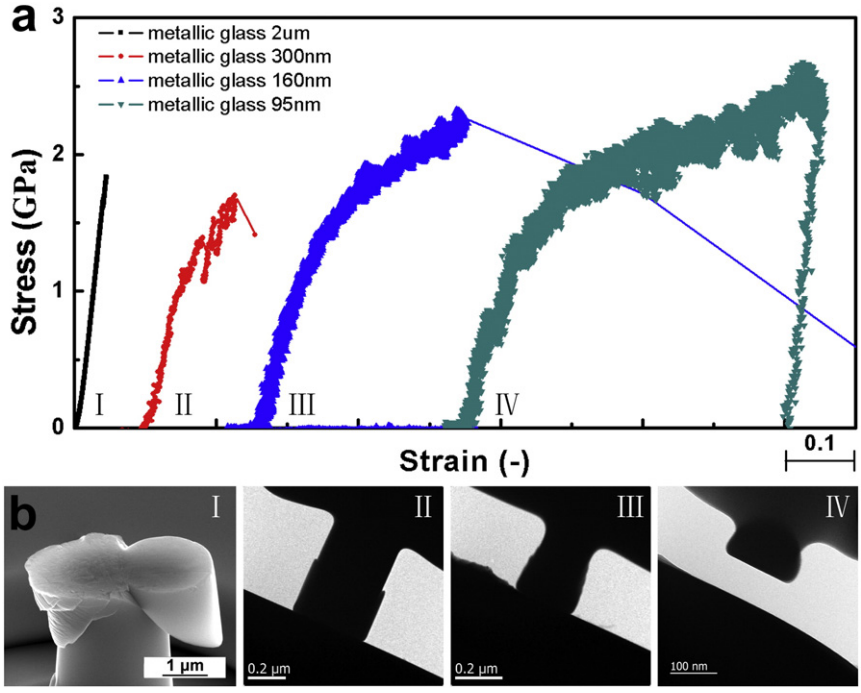

Fig. 2. (a) The compressive stress–strain curves of $Sc_{75}Fe_{25}$ metallic glass pillars. (b) The frames of (I) 2 μm; (II) 300 nm; (III) 160 nm; (IV) 95 nm metallic glass pillar, respectively, are extracted from recorded movies.

the tendency for localized shear. In other words, the reduction of sample size results in a more uniform deformation mode, elevated strength and enhanced plasticity.

Compressive yield strengths as a function of sample size for $Sc_{75}Fe_{25}$ nanoglass and metallic glass are shown in Fig. 3. The yield strength of the metallic glass sample slightly increased as the sample size was decreased. Simultaneously, the deformation mode changed from inhomogeneous deformation to uniform deformation around 300 nm. In the case of $Sc_{75}Fe_{25}$ nanoglass, the existence of a large number of interfaces seems beneficial for the nucleation and the subsequent multiplication of shear bands. On the other hand, the yield strength is still controlled by shear band propagation [10]. As a consequence, the yield strength of the nanoglass samples varies little with the sample size. However, when the sample size was reduced to less than 100 nm, the shear banding thickness (10–20 nm) [20] became comparable to the sample

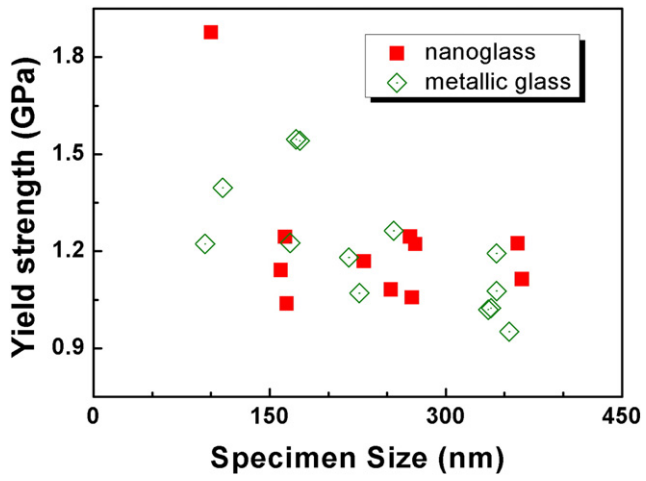

Fig. 3. Compression yield strengths as a function of sample size for $Sc_{75}Fe_{25}$ nanoglass and $Sc_{75}Fe_{25}$ metallic glass, respectively.

size, the yield strength and deformation mechanism changed significantly (Fig. 3). Indeed, individual shear bands can be identified in Fig. 1b(III) and uniform deformation can be observed in Fig. 1b(IV). This change of the deformation mode is analogous to the strain burst related to the movement of discrete dislocations in single crystals with a micro-scale size [5].

It has been recognized that plastic flow of metallic glasses occurs as a result of a series of flow defects that are nucleated preferentially at larger free volume sites [21–23], and these processes tend to further increase the local free volume (free volume creation), giving rise to auto-catalytic shear softening. As deformation proceeds, flow defects interact elastically in the long range as well as configurationally in the short range, and begin to self-organize in a hierarchical manner. As a flow defects get larger in volume under stress, its aspect ratio also tends to increase due to the nature of shear elastic interaction [24]. An embryonic shear band is defined as a flow defect with a long aspect ratio. Inside the embryonic shear band, there is always shear softening due to free-volume generation and later heating through elastic energy release [25,26]. This drives the forward propagation and elongation of the same embryonic shear band, with increasing aspect ratio. When a critical incubation size scale l_{inc} is reached, the embryonic shear band will develop into a mature shear band (Fig. 4a). Subsequently, there is so much softening, energy release concentration and heating in one major shear band that cavitations occur inside, leading to fracture along its shear plane [24]. This is most likely the reason that 2 μm pillar and 300 nm pillar fail by shear along the plane of the major shear band.

When the sample size was decreased from 300 nm to 95 nm, the results reported above reveal that the yield strength for the metallic glass becomes size-dependent in the sense that the yield strength increases when the sample size is reduced. Simultaneously, the deformation mode changed from inhomogeneous deformation (shear banding) to uniform deformation as is shown in both the stress–strain curves and the micrographs of the free surfaces. These results agree with several recent reports suggesting that some metallic glasses displayed a transition from an inhomogeneous to homogeneous deformation mode when the sample size was reduced to submicron scale [9,11,14,15,27,28]. The sample size (~300 nm) observed in our experiments for such a

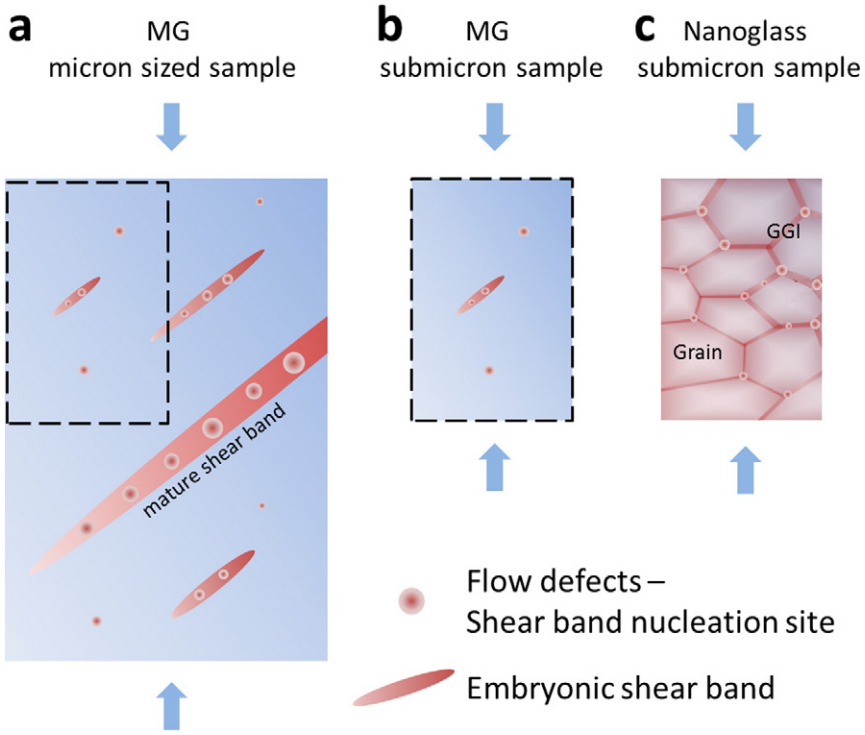

Fig. 4. Schematic representation of shear band nucleation for metallic glass and nanoglass. (a) As the requirements for quantity and orientations have been met, a series of flow defects will develop into a mature shear band in MG sample, (b) for submicron MG sample, there is not enough free space among the shear band nuclei for growing into a mature shear band, (c) for nanoglass, the existence of a large number of GGIs benefits for shear band nucleation and the subsequent multiple shear banding.

transition is consistent with previous investigations for some MG systems [9,15]. However, when the sample size was reduced down to 100 nm or below, which is comparable to critical incubation size scale l_{inc}, there is not enough free space between the shear band nuclei for growing into a mature shear band (Fig. 4b). In other words, shear band nucleation becomes difficult. Therefore, many embryonic shear bands will form simultaneously, resulting in homogeneous plastic deformation. In fact, the 95 nm pillar deformed uniformly due to the movement of shear transformation zones (STZ)/diffusion, which suggests that shear bands are difficult to nucleate and uniform deformation becomes dominant. For metallic glasses, the change in deformation mode from more inhomogeneous to homogeneous may be attributed to shear band nucleation starvation. Shear band nucleation starvation mechanism might be analogous to the dislocation source starvation [5,6,29] in micro-scale single crystals.

In the case of the nanoglass, the yield strength is size-independent and the deformation mode remains multiple shear-banding. As is evidenced by shear offsets at the sample surfaces and the stress drops in deformation curves, the yield strength of the nanoglass is controlled by shear band propagation [4,10]. Owing to an enhanced free volume and an increased potential energy [4,16] in GGIs, shear in the nanoglass initiates at these regions. The propagation of the GGI flow defect will be impeded by the glassy grains. Plastic flow then will take place in other sites, resulting in significant global plastic strain (Fig. 4c). As a consequence, the existence of a large number of GGIs in the nanoglass benefits for the nucleation and the subsequent multiplication of shear bands while the metallic glass is shear band nucleation starved in samples of small sizes [4,30–32]. As is observed above in the experimental section, the transition of deformation mode in nanoglasses might occur at a smaller size scale (~100 nm).

In summary, the mechanical properties of small scaled $Sc_{75}Fe_{25}$ nanoglass and metallic glass were investigated by means of compression tests. Yield strength and multiple shear banding were found to be size-independent in $Sc_{75}Fe_{25}$ nanoglass, whereas it is not the case in the melt-spun metallic glass. The former should be attributed to the high density of glass/glass interfaces acting as effective sites for shear band nucleation. The later is owing to the reduced nucleation sites for shear band nucleation in MGs resulting in the observed size dependence of the yield strength and deformation mechanism.

Supplementary data to this article can be found online at http://dx.doi.org/10.1016/j.scriptamat.2016.01.036.

Acknowledgments

The authors acknowledge the financial support from the National Natural Science Foundation of China (NSFC) under Grant Nos. 51171138, 51171139, and 51321003 and Ph.D. J.L. acknowledges the support by NSF DMR-1120901 and DMR-1410636. HH and HG are grateful to the Deutsche Forschungsgemeinschaft under Grant HA 1344/30-1 of the SPP1594 program. The authors are also grateful for the support from Center for Advancing Materials Performance from the Nanoscale (CAMP-Nano).

References

[1] J. Jing, A. Krämer, R. Birringer, H. Gleiter, U. Gonser, J. Non-Cryst. Solids 113 (1989) 167–170.
[2] J.Q. Wang, N. Chen, P. Liu, Z. Wang, D.V. Louzguine-Luzgin, M.W. Chen, J.H. Perepezko, Acta Mater. 79 (2014) 30–36.
[3] N. Chen, X. Shi, R. Witte, K.S. Nakayama, K. Ohmura, H. Wu, A. Takeuchi, H. Hahn, M. Esashi, H. Gleiter, A. Inoue, D.V. Louzguine, J. Mater. Chem. B 1 (2013) 2568.
[4] X.L. Wang, F. Jiang, H. Hahn, J. Li, H. Gleiter, J. Sun, J.X. Fang, Scr. Mater. 98 (2015) 40–43.
[5] M.D. Uchic, D.M. Dimiduk, J.N. Florando, W.D. Nix, Science 305 (2004) 986–989.
[6] J.R. Greer, W.C. Oliver, W.D. Nix, Acta Mater. 53 (2005) 1821–1830.
[7] J.R. Greer, J.T.M. De Hosson, Prog. Mater. Sci. 56 (2011) 654–724.
[8] Z.J. Wang, Q.J. Li, Z.W. Shan, J. Li, J. Sun, E. Ma, Appl. Phys. Lett. 100 (2012).
[9] C.A. Volkert, A. Donohue, F. Spaepen, J. Appl. Phys. 103 (2008) 083539.
[10] C.C. Wang, J. Ding, Y.Q. Cheng, J.C. Wan, L. Tian, J. Sun, Z.W. Shan, J. Li, E. Ma, Acta Mater. 60 (2012) 5370–5379.
[11] D.C. Jang, J.R. Greer, Nat. Mater. 9 (2010) 215–219.
[12] D.C. Jang, C.T. Gross, J.R. Greer, Int. J. Plast. 27 (2011) 858–867.
[13] A. Dubach, R. Raghavan, J. Loffler, J. Michler, U. Ramamurty, Scr. Mater. 60 (2009) 567–570.

[14] C.Q. Chen, Y.T. Pei, O.V. Kuzmin, Z.F. Zhang, E. Ma, J.T.M. De Hosson, Phys. Rev. B 83 (2011).
[15] O.V. Kuzmin, Y.T. Pei, C.Q. Chen, J.T.M. De Hosson, Acta Mater. 60 (2012) 889–898.
[16] J.X. Fang, U. Vainio, W. Puff, R. Würschum, X.L. Wang, D. Wang, M. Ghafari, F. Jiang, J. Sun, H. Hahn, H. Gleiter, Nano Lett. 12 (2012) 458–463.
[17] W.J. Wright, R. Saha, W.D. Nix, Mater. Trans. 42 (2001) 642–649.
[18] W. Klement, R.H. Willens, P. Duwez, Nature 187 (1960) 869–870.
[19] A.L. Greer, Y.Q. Cheng, E. Ma, Mater. Sci. Eng. R. Rep. 74 (2013) 71–132.
[20] Y. Zhang, A.L. Greer, Appl. Phys. Lett. 89 (2006) 071903–071907.
[21] W. Johnson, K. Samwer, Phys. Rev. Lett. 95 (2005).
[22] M.L. Falk, Phys. Rev. B (1999) 7062–7070.
[23] M.L. Falk, J.S. Langer, Phys. Rev. E 57 (1998) 7192.
[24] P.Y. Zhao, J. Li, Y.Z. Wang, Int. J. Plast. 40 (2013) 1–22.
[25] F. Shimizu, S. Ogata, J. Li, Acta Mater. 54 (2006) 4293–4298.
[26] M.Q. Jiang, L.H. Dai, Acta Mater. 59 (2011) 4525–4537.
[27] H. Guo, P.F. Yan, Y.B. Wang, J. Tan, Z.F. Zhang, M.L. Sui, E. Ma, Nat. Mater. 6 (2007) 735–739.
[28] L. Tian, Z.W. Shan, E. Ma, Acta Mater. 61 (2013) 4823–4830.
[29] Z.W. Shan, R.K. Mishra, S.A. Syed Asif, O.L. Warren, A.M. Minor, Nat. Mater. 7 (2008) 115–119.
[30] L. Yao, Z.H. Jin, Scr. Mater. 106 (2015) 46–51.
[31] Z.D. Sha, P.S. Branicio, Q.X. Pei, Z.S. Liu, H.P. Lee, T.E. Tay, T.J. Wang, Nanoscale 7 (2015) 17404–17409.
[32] S. Adibi, P.S. Branicio, S.P. Joshi, Sci. Report. 5 (2015) 15611.